Myosin-X Silencing in the Trabecular Meshwork Suggests a Role for Tunneling Nanotubes in Outflow Regulation

Ying Ying Sun, Yong-Feng Yang, and Kate E. Keller

Casey Eye Institute, Oregon Health & Science University, Portland, Oregon, United States

Correspondence: Kate E. Keller, Casey Eye Institute, Oregon Health & Science University, 3181 SW Sam Jackson Park Road, Portland, OR 97239, USA; gregorka@ohsu.edu.

Submitted: October 26, 2018
Accepted: January 25, 2019

Citation: Sun YY, Yang Y-F, Keller KE. Myosin-X silencing in the trabecular meshwork suggests a role for tunneling nanotubes in outflow regulation. *Invest Ophthalmol Vis Sci*. 2019;60:843–851. https://doi.org/10.1167/iovs.18-26055

Purpose. The actin cytoskeleton plays a key role in outflow regulation through the trabecular meshwork (TM). Although actin stress fibers are a target of glaucoma therapies, the role of other actin cellular structures is unclear. Myosin-X (Myo10) is an actin-binding protein that is involved in tunneling nanotube (TNT) and filopodia formation. Here, we inhibited Myo10 pharmacologically or by gene silencing to investigate the role of filopodia/TNTs in the TM.

Methods. Short hairpin RNA interference (RNAi) silencing lentivirus targeting myosin-X (shMyo10) was generated. Human anterior segments were perfused with shMyo10 or CK-666, an Arp2/3 inhibitor. Confocal microscopy investigated the colocalization of Myo10 with matrix metalloproteinase (MMPs). Western immunoblotting investigated the protein levels of MMPs and extracellular matrix (ECM) proteins. MMP activity and phagocytosis assays were performed.

Results. CK-666 and shMyo10-silencing lentivirus caused a significant reduction in outflow rates in anterior segment perfusion culture, an ex vivo method to study intraocular pressure regulation. In human TM cells, Myo10 colocalized with MMP2, MMP14, and cortactin in podosome-like structures, which function as regions of focal ECM degradation. Furthermore, MMP activity, thrombospondin-1 and SPARC protein levels were significantly reduced in the media of CK-666-treated and shMyo10-silenced TM cells. However, neither Myo10 silencing or CK-666 treatment significantly affected phagocytic uptake.

Conclusions. Inhibiting filopodia/TNTs caused opposite effects on outflow compared with inhibiting stress fibers. Moreover, Myo10 may also play a role in focal ECM degradation in TM cells. Our results provide additional insight into the function of actin supramolecular assemblies and actin-binding proteins in outflow regulation.

Keywords: trabecular meshwork, actin cytoskeleton, extracellular matrix, aqueous humor dynamics

Intraocular pressure (IOP) is established by building a resistance to aqueous humor outflow in the juxtacanalicular region of the trabecular meshwork (TM) and inner wall endothelium of Schlemm's canal (SC).[1] Dysfunction in the aqueous outflow channels causes elevated IOP, which eventually causes glaucomatous damage to the optic nerve and loss of vision.[2] TM cells detect changes in IOP as a mechanical stretch, which activate integrins and induce several intracellular signaling pathways that result in TM cells releasing enzymes, such as matrix metalloproteinases (MMPs) to remodel the extracellular matrix (ECM). This allows greater fluid drainage from the anterior chamber to alleviate elevated IOP.[3]

The actin cytoskeleton of TM cells is also important for IOP regulation. Activity of the small Rho GTPases, Rho, rac1, and cdc42, gives rise to stress fibers, lamellipodia, and filopodia, respectively.[3] Several studies have demonstrated that drugs that either inhibit polymerization of actin into stress fibers or depolymerize actin stress fibers increase outflow facility ex vivo and in vivo.[4–11] A Rho kinase inhibitor, Netarsudil, has recently been approved as a new drug to reduce elevated IOP in glaucoma patients.[12] Although these studies have elegantly demonstrated the critical role of stress fibers in IOP regulation, the role of other actin-based cellular structures in IOP regulation is largely unknown. Lamellipodia are characteristic of migratory cells, such as cancer cells, and are not typically associated with sedentary TM cells. However, many dynamic filopodia decorate the surface of TM cells.[13]

Filopodia are long, thin protrusions that emanate from the cell surface to probe their mechanical environment.[14] Filopodia contain tight bundles of filamentous (F)-actin and arise from the Arp2/3-generated branched actin networks that lie just beneath the plasma membrane.[15] Two filopodia arising from adjacent cells can fuse to form a connecting tube, which are called tunneling nanotubes (TNTs).[16–18] These TNTs function in cellular communication and transport a variety of cargoes, including viruses, microRNAs, and cellular organelles such as endosomes, lysosomes, and mitochondria. We recently described TNT formation by TM cells.[13] This direct method of cellular communication overcomes limitations of diffusion-based signaling in the aqueous environment of the anterior chamber. Thus, filopodia have multiple important functions, such as sensing biomechanical signals, acting as sites for signal transduction, as well as communicating signals via the formation of TNTs.

Myosin-X (Myo10) is an unconventional myosin, which functions in filopodia and TNT formation.[19,20] It comprises an N-terminal head domain, which binds to F-actin and moves cargo, bound to the C-terminal tail domain, toward the tip of

the filopodia.[21] Thus, Myo10 tends to accumulate at the tips of filopodia.[22] Myo10 appears to function in filopodia formation because GFP-Myo10 rapidly accumulates at sites of filopodia initiation and overexpression of Myo10 led to a massive increase in the number of dorsal filopodia.[20,23] Conversely, RNA interference (RNAi) silencing or knockout of Myo10 drastically reduces the number of filopodia or shortens those filopodia that do form.[19,24] Other studies show that Myo10 is essential for TNT formation.[19] Myo10 localizes to other cellular structures displaying dynamic actin reorganization, such as invadopodia, podosomes, phagocytic cups, and the leading edges of lamellipodia.[25–28] The role of Myo10 in the TM is unknown. However, Myo10 mRNA expression increased in cells subject to cyclical mechanical stress, which mimics IOP fluctuations.[29] Myo10 appears to play a role in ECM degradation because there were lower levels of active MMP9 and MMP14 in a Myo10-silenced human breast adenocarcinoma cell line.[28,30] Other reports show that Myo10 binds integrins, which may be important for phagocytosis.[26,31]

In this study, we investigated the function of Myo10 in the TM. We used two methods to inhibit filopodia and TNT formation: (1) CK-666, a reversible Arp2/3 inhibitor, which disrupts formation of branched actin networks from which filopodia arise[15,32,33]; and (2) generated short hairpin RNAi silencing lentivirus targeting *MYO10* (shMyo10). The effects of CK-666 and shMyo10 on outflow rates in anterior segment perfusion culture were measured as well as the role of Myo10 in ECM remodeling and phagocytosis by TM cells.

Methods

TM Cell Culture

Human TM cells were established from cadaver tissue and cultured following the guidelines recently described.[34] Demographics of the human donors are found in Supplementary Table S1, and Western immunoblots confirming induction of myocilin following 14 days of dexamethasone treatment are shown in Supplementary Figure S1. The following experiments were performed using 3 to 5 different cell strains for each assay.

Generation of Myo10 Silencing Lentivirus

Short hairpin RNAi lentivirus targeting Myo10 was generated as previously described.[35] Short hairpin RNAs (ShRNAs) were designed using the online BLOCK-iT RNAi designer (ThermoFisher, Waltham, MA, USA). The 21-base pair (bp) target sequence 5′-GGTTTGTACTCACCCACAATT-3′ targeted the human Myo10 gene. A shRNA control (shCtrl) was previously characterized.[35,36] Hairpin primers were annealed and cloned into the pENTR/U6 vector, which contained a human U6 promoter and an RNA polymerase III terminator, using T4 ligase. After DNA sequencing, shRNA cassettes were transferred into the pLenti6/BLOCK-iT-DEST vector by recombination using the Gateway LR clonase II enzyme. Replication incompetent lentivirus was generated in the 293FT cell line by cotransfecting the pLenti expression plasmid with ViraPower packaging mix using Lipofectamine 2000. Lentiviral-containing supernatants were harvested 72 hours posttransfection and centrifuged at 85,000*g* in a L-80 ultracentrifuge (Becman Coulter Life Sciences, Indianapolis, IN, USA) with a SW28.1 rotor for 2 hours, and viral titers were measured. Viral supernatants were then aliquoted and stored at –80°C until use.

To quantitate Myo10 gene knockdown, human TM cells or 293 cells were transduced with 10^6 plaque-forming units (PFUs) of shMyo10 and shCtrl lentivirus for 48 hours. Total RNA was isolated using cells-to-cDNA lysis buffer (ThermoFisher) and quantitative RT-PCR was performed using Myo10-specific primers (5′-CGGATGTGGTGGAACAGATTTA-3′ and 5′-CAATAATCCAGGGCATCCTACAG-3′). Results were normalized to 18S RNA as a housekeeping gene and expressed as fold-change relative to shCtrl-transduced cells. Significance was determined by ANOVA. To analyze Myo10 protein, RIPA lysates of shMyo10-silenced cells were subject to Western immunoblotting with Myo10 rabbit polyclonal antibody (HPA024223; MilliporeSigma, St Louis, MO, USA). Densitometry (FIJI software; http://fiji.sc/Fiji, provided in the public domain) was used to measure band intensity and determine the percentage knockdown of shMyo10 compared to shCtrl-transduced cells.

Anterior Segment Perfusion Culture

The average age of human cadaver eyes used for perfusion experiments was 77.9 ± 7.9 years (range, 59–90) (Supplementary Table S1). Human eyes were dissected and anterior segments were clamped into a perfusion chamber and perfused at constant pressure (8 mm Hg) with serum-free Dulbecco's Modified Eagles Medium.[37] Anterior segments that could not be stabilized were discarded. After overnight stabilization of flow rates, 100 μM CK-666[32,33] or 0.04% dimethyl sulfoxide (DMSO) control, or 1 ml (10^6 PFUs) shMyo10 or shCtrl lentivirus,[35,36] was added as a bolus at time point 0. Flow rates were measured twice a day for a further 70 to 75 hours. For each individual perfused eye, outflow rates after treatment were normalized to the average flow rate before treatment. Data from multiple eyes were then averaged, and a standard error of the mean was calculated. ANOVA was used to determine significance.

At the end of perfusion, the anterior segments were fixed in 4% paraformaldehyde. The tissue was cut then into approximately 10 to 12 wedges and embedded into paraffin, and 5-μm radial sections were cut at the histopathology core facility (Knight Cancer Institute, Oregon Health & Science University, Portland, OR, USA). After deparaffinization and rehydration, the sections were blocked and stained with rabbit anti-Myo10 polyclonal antibodies. Primary antibodies were detected with Alexa fluor 594-conjugated goat anti-rabbit secondary antibodies (ThermoFisher). Coverslips were mounted in ProLong gold mounting medium containing 4′,6-diamidino-2-phenylindole (DAPI), and sections were imaged on an Olympus Fluoview confocal microscope (Olympus, Waltham, MA, USA). Open-source FIJI software was used to process images postcapture.

Western Immunoblotting

Human TM cells (Supplementary Table S1) were grown to confluence, washed with phosphate-buffered saline (PBS), placed into serum-free medium, and treated with 100 μM CK-666 or 0.04% DMSO (vehicle) for 24 hours.[32] Serum-free medium was collected, and the total amount of protein in each sample was quantitated using a bicinchoninic acid (BCA) protein assay (Pierce, Rockford, IL, USA). Equal amounts of total protein were loaded on the gel, and proteins were separated by SDS-PAGE (BioRad Labs, Hercules, CA, USA) under reducing conditions. Primary antibodies were fibronectin (FN) mouse monoclonal (610077, clone 10; BD Biosciences, San Jose, CA, USA), tenascin C (TNC) rabbit polyclonal (AB19011; MilliporeSigma), collagen type I and collagen type IV mouse monoclonal (M-38 and M3F7; Developmental Studies Hybridoma Bank, University of Iowa, Iowa City, IA, USA), secreted protein acidic and rich in cysteine (SPARC) rabbit polyclonal (15274-1-AP; Proteintech Group, Rosemont, IL,

USA), and thrombospondin-1 (TSP-1) mouse monoclonal (MA1-26372, clone A6.1; ThermoFisher). Secondary antibodies were IRDye 700-conjugated anti-rabbit and IRDye 800-conjugated anti-mouse (Rockland Immunochemicals, Gilbertsville, PA, USA). Membranes were imaged on the Odyssey gel imaging system (Licor, Lincoln, NE, USA). The intensity of each band was determined by densitometry using FIJI software, and experimental data are presented as a percentage of the untreated control. Results show the average ± standard error of the mean of four technical replicates using TM cell strains derived from three biological replicates.

Immunofluorescence and Confocal Microscopy

Human TM cells were plated on collagen type I-coated Bioflex 6-well plates (FlexCell International Corp. Burlington, NC, USA) and treated for 24 hours with 100 μM CK-666 or 0.04% DMSO vehicle control.[32] Immunofluorescence and confocal microscopy were performed as detailed previously.[38,39] Primary antibodies were rabbit polyclonal anti-myosin-X (PA5-55019, ThermoFisher; or AAS09642C, Antibody Verify, Las Vegas, NV, USA), mouse monoclonal anti-MMP2 (MAB3308; MilliporeSigma), mouse monoclonal anti-MMP14 (MAB3319; MilliporeSigma), and mouse anti-cortactin p80/85 (05-180; MilliporeSigma). At least three TM cell strains were used.

MMP Assay

MMP activity was measured using the SensoLyte 520 generic MMP assay kit and the SensoLyte 520 Aggrecanase-1 assay kit (Anaspec, Inc., Fremont, CA, USA).[40,41] Briefly, confluent human TM cells were placed in serum-free medium and treated with 100 μM CK-666 or 0.04% DMSO. For shMyo10, TM cells were transduced at the time of plating, grown for 72 hours, and then swapped into serum-free medium. Media and cell lysates were collected 24 hours later. MMPs in each sample were activated with 1 mM 4-aminophenylmercuric acetate for 90 minutes at 37°C. Samples were incubated with QXL520-quenched 5-fluoroscein amidite (FAM)-labeled fluorescent substrate. Active MMPs cleaved the quencher, and 5-FAM fluorescence was measured on a plate reader (excitation/emission = 490/520 nm). Relative fluorescence units were normalized to total protein in each sample, as determined using a BCA assay. Each sample was measured in duplicate, then the data from three biological replicates were averaged, and a standard error of the mean was calculated.

Phagocytosis Assay

To measure phagocytosis, pHrodo *Staphylococcus aureus* fluorescent bioparticles (1 mg/ml; ThermoFisher) were resuspended in PBS and vortexed to disperse, and 50 μl of opsonizing reagent (ThermoFisher) was added. The solution was incubated at 37°C for 1 hour. After washing, the pellet was resuspended in PBS. TM cells were plated in 6-well plates (CytoOne; USA Scientific, Ocala, FL, USA) in the presence of shMyo10 silencing lentivirus for 3 days and placed into fresh medium prior to the start of the experiment. For CK-666, TM cells at 70% confluence were pretreated for 2 hours with 100 μM CK-666 in DMSO. Controls included shCtrl silencing lentivirus, 0.04% DMSO vehicle control ,and pretreatment for 30 minutes with 0.78 μM cytochalasin D to disrupt the actin cytoskeleton. Opsonized pHrodo BioParticles (100 μl) were added to each well, and the plate was placed in the Incucyte ZOOM instrument (Essen Bioscience, Ann Arbor, MI, USA). Each well was imaged at 9 points, every 15 minutes for 16 hours using the phase and red fluorescence channels and the 20× objective. At the end of the experiment, the fluorescence intensity at each time point in each well was measured using FIJI. This phagocytosis assay was repeated three times using three biological replicates. Data were combined and averaged and a standard error calculated.

Statistical Analyses

The number of biological and technical replicates are stated in the figure legends. Data are presented as the average ± standard error of the mean. Significance was determined using ANOVA and when needed with Bonferroni correction. $P < 0.05$ was considered statistically significant.

Results

Transduction of human TM cells with shMyo lentivirus showed a 45% reduction in *MYO10* mRNA levels (Fig. 1A) and Myo10 protein levels were reduced approximately 25% (Figs. 1B, 1C). By immunofluorescence and confocal microscopy, Myo10 displayed a more punctate distribution pattern in shMyo10-silenced TM cells compared to shCtrl-transduced cells (Figs. 1D, 1E).

CK-666 is a reversible inhibitor of the Arp2/3 complex, which is important for assembly of branched actin networks from which filopodia arise.[32] To test the effects of outflow, we applied CK-666 or shMyo10 lentivirus to anterior segment perfusion culture, an established ex vivo method to study IOP regulation.[37] Human cadaver anterior segments were perfused with a bolus of 100 μM CK-666 (Fig. 2A). At 2 to 4 hours after CK-666 application, flow rates were significantly reduced by approximately 45% compared to DMSO vehicle controls. Flow rates then recovered toward baseline, followed by another 45% decrease in outflow between 50 and 76 hours after application (Fig. 2A) ($P < 0.05$). In anterior segments that were perfused with shMyo10 lentivirus, there was an approximately 40% reduction in outflow rates compared to a control lentivirus from approximately 4 hours, which was sustained throughout the perfusion experiment (Fig. 2B) ($P < 0.05$). Postperfusion, TM tissue sections from all quadrants of each eye were stained with hematoxylin and eosin (Figs. 2C, 2E, 2G) or immunostained with Myo10 (Figs. 2D, 2F, 2H). Hematoxylin and eosin staining showed no discernible differences in tissue architecture or cell number between CK-666-treated, shMyo10-transduced, and their controls. In Myo10-silenced TM, Myo10 protein was decreased as expected and the distribution pattern was altered. A negative control section, where the primary antibody was substituted by PBS, is shown in Supplementary Figure S2.

Studies in other cell types suggest that Myo10 may play a role in ECM degradation. Myo10 is localized to podosomes in osteoclasts and MMP9 mRNA is downregulated, and proteinase activity is reduced when Myo10 is silenced in breast cancer tumors.[25,28,30] In TM cells, we previously described cellular structures called podosome and invadosome-like structures, which are regions of a TM cell important for focal ECM degradation.[42] Therefore, we compared the cellular localization of Myo10 in regard to MMPs and tested the effects of shMyo10 and CK-666 on MMP activity. We localized Myo10 to ring-like structures that were similar in shape and size to podosome rosettes (5-μm diameter) and podosome clusters (10–15 μm) (Fig. 3A).[42,43] To confirm this, we colocalized Myo10 with cortactin antibodies, a biomarker of podosomes (Fig. 3B). Next, we colocalized Myo10 with the MMPs MMP2 and MMP14 (Figs. 3C, 3D). In areas of presumptive podosomes, there was strong colocalization (yellow) of Myo10 with MMP2 (Fig. 3C) and MMP14 (Fig. 3D) whereas there was little colocalization in other cellular areas.

Investigative Ophthalmology & Visual Science

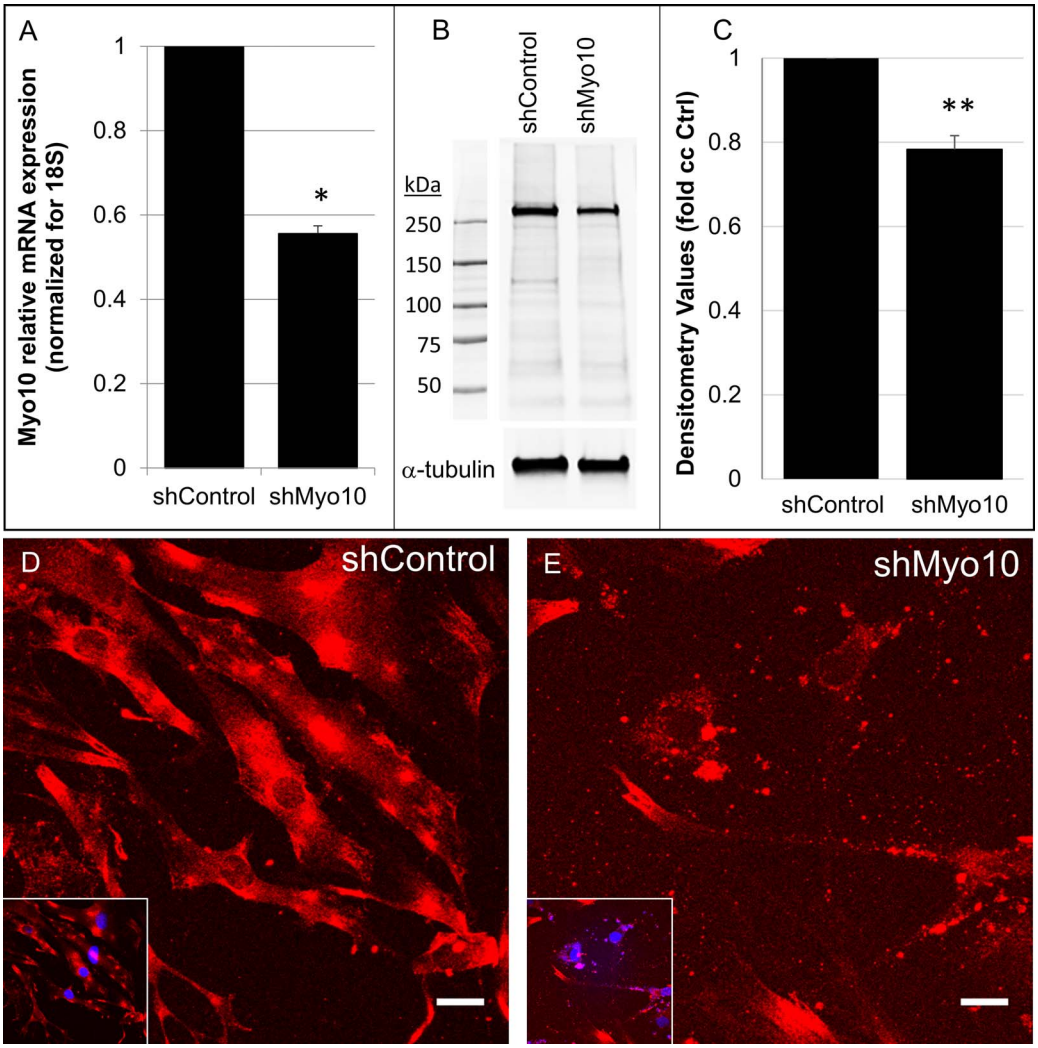

Figure 1. Generation of shRNA Myo10-silencing lentivirus (shMyo10) silencing lentivirus. Efficacy of Myo10 knockdown in human TM cells by infection with shMyo10-silencing lentivirus was tested by (**A**) quantitative RT-PCR using Myo10-specific primer sets. $^{*}P = 0.0001$; $n = 4$ from 4 biological replicates. (**B**) Western immunoblotting of Myo10 with tubulin as a loading control and (**C**) densitometry of Myo10 knockdown. $^{**}P = 0.001$; $n = 7$ from 5 biological replicates. Immunofluorescence of Myo10 in (**D**) shCtrl and (**E**) shMyo10-silenced human TM cells. Insets show DAPI staining. *Scale bar:* 20 μm.

Next, we quantitated MMP activity using a fluorogenic MMP assay using a quenched peptide that generates fluorescence following cleavage of MMPs in the sample. We used a substrate specific for ADAMTS4, as well as a substrate that is cleaved by several MMPs.[40] There was no apparent difference in MMP or ADAMTS4 activities in cell lysates from CK-666-treated or Myo10-silenced TM cells (Fig. 3E). However, MMP activity in TM cell medium was significantly reduced by 25% and 58% by CK-666 and shMyo10, respectively. We also investigated protein levels of MMP2 and MMP14 in TM cell lysates and serum-free medium from TM cells treated for 24 hours with CK-666 or transduced with shMyo10 (Fig. 3F). Densitometry showed a significant ~25% decrease in MMP14 of shMyo10-silenced TM cells and a ~15% decrease in MMP2 levels in CK-666-treated TM cells.

A critical component of ECM remodeling is the synthesis of new ECM to replace the degraded matrix.[44] Therefore, we also investigated the levels of ECM components synthesized by TM cells in response to the treatments. We focused on ECM proteins that either have structural roles (e.g., collagen types I and IV), cell adhesion (e.g., FN), or ECM organizational roles (e.g., TNC, SPARC, and TSP-1).[45,46] CK-666 was added to TM cells in culture, and serum-free medium was collected 24 hours later. Western immunoblotting and densitometry showed that there was no significant difference in the protein levels for FN, TNC, and collagens type I or type IV (Fig. 4A). However, TSP-1 protein levels were significantly reduced ($P < 0.05$), and SPARC levels were also reduced, although this just missed significance ($P = 0.065$) (Fig. 4B). SPARC was significantly reduced following shMyo10 silencing, whereas TSP-1 was reduced but not significantly (Fig. 4C). Together, these results suggest that inhibition of filopodia/TNTs decreases ECM degradation and alters the composition of the replacement ECM synthesized.

Other studies have shown that Myo10 is localized to phagocytic cups.[26] Because TM cells are phagocytic, we investigated the effects of CK-666 and shMyo10 silencing on phagocytosis by TM cells. To measure phagocytosis, pHrodo *S. aureus* fluorescent bioparticles were used. These dramatically increase fluorescence when they are ingested and exposed to the intracellular acidic environment of the phagosome. Fluorescence intensity was measured over time for TM cells

Investigative Ophthalmology & Visual Science

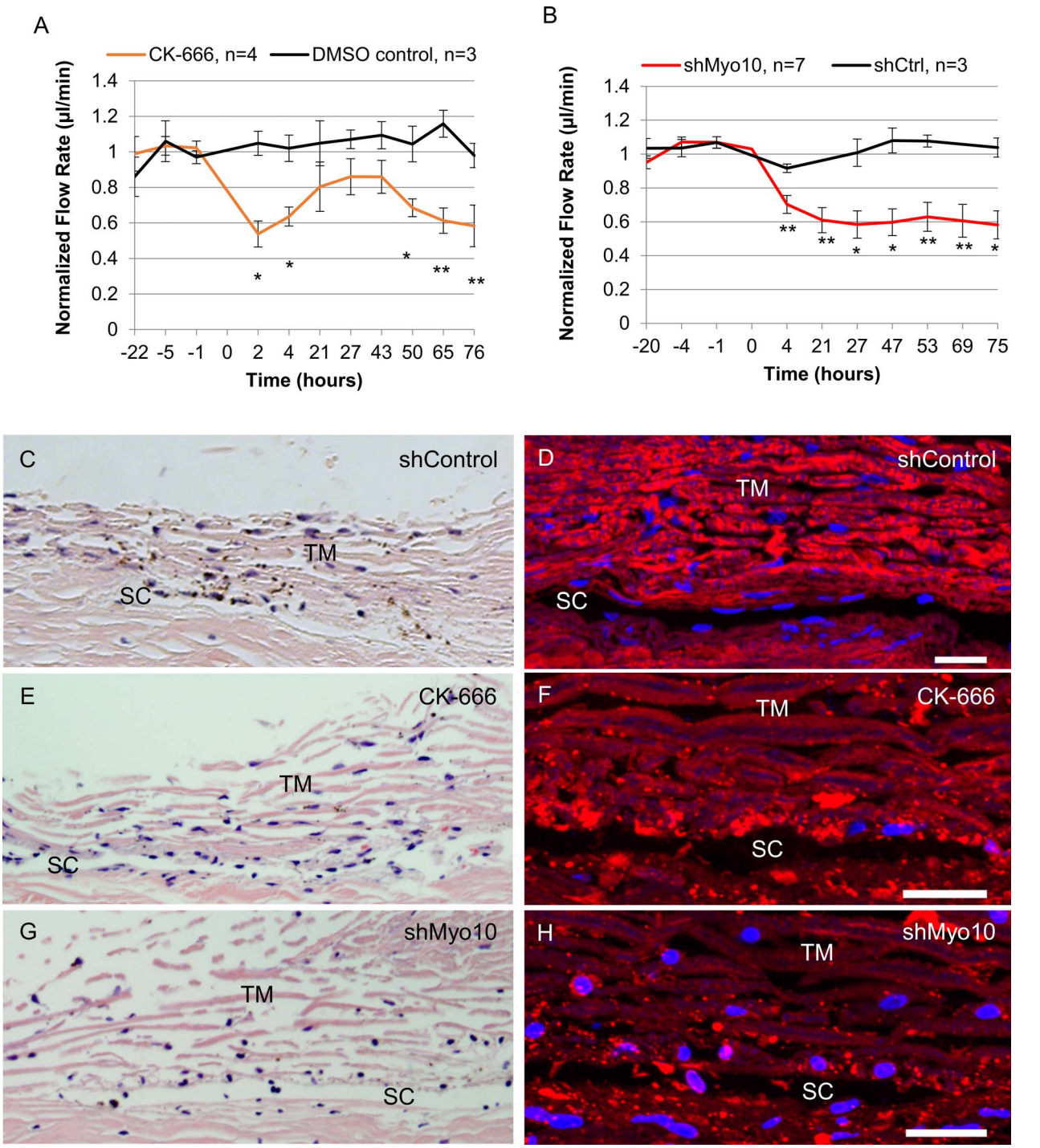

Figure 2. Human anterior segment perfusion culture. Following baseline stabilization, treatments were applied at time point 0 as follows: (**A**) a bolus of 100 µM CK-666 ($n = 4$) or 0.04% DMSO vehicle control ($n = 3$), or (**B**) shRNA Myo10-silencing lentivirus (shMyo10; $n = 7$) or shControl (shCtrl; $n = 3$). Flow rate data at each time point were normalized to the average flow rate before treatment. Data from individual eyes were then averaged. *Error bars* are the SEM. $^{*}P < 0.01$, $^{**}P < 0.05$ by ANOVA. (**C**) Representative radial sections of TM tissue postperfusion stained with hematoxylin and eosin (**C**, **E**, **G**), or immunostained with anti-Myo10 (*red*; **D**, **F**, **H**). DAPI stained nuclei *blue*. TM, trabecular meshwork; SC, Schlemm's canal. *Scale bar:* 20 µm.

transduced with shMyo10-silencing lentivirus and for TM cells treated with CK-666. There was no significant difference in phagocytic activity of TM cells at any time point with either treatment compared to their respective controls (Figs. 5A, 5B). Representative images of the phagocytosis assay are also shown (Fig. 5C).

Discussion

In this study, we investigated the role of the actin-binding protein Myo10 in outflow regulation. Although both CK-666 and Myo10 silencing decreased outflow in perfusion culture, there were differences in the outflow effects caused by the two

Investigative Ophthalmology & Visual Science

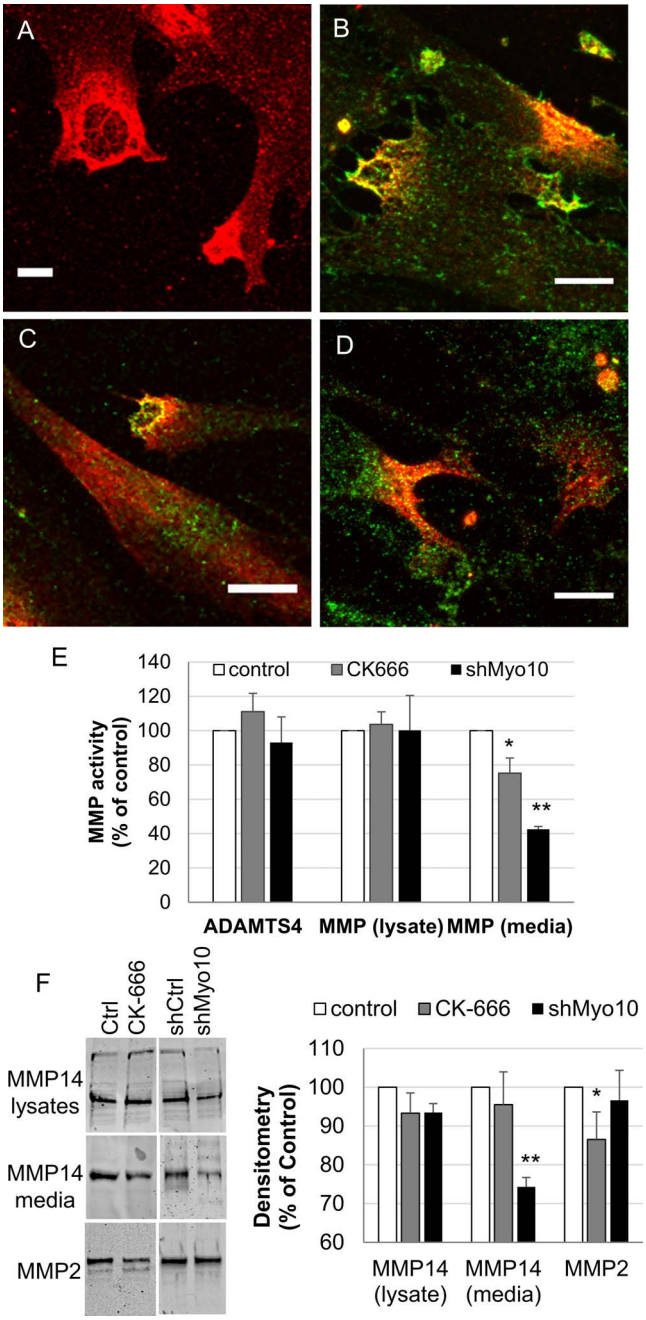

FIGURE 3. Effects of filopodia/TNT inhibition on MMP activity by TM cells. (**A**) Myo10 localizes to podosome-like structures in human TM cells, where is partially colocalizes with (**B**) cortactin, a podosome biomarker, (**C**) MMP2, and (**D**) MMP14. *Scale bars* = 10 µm. (**E**) ADAMTS4 and MMP activity assays of human TM cells treated with CK-666 or shMyo10-silenced TM cells. MMP activity in the medium was significantly reduced by CK-666 (compared to DMSO vehicle) and shMyo10 (compared to shCtrl). $^{*}P = 0.048$, $^{**}P = 0.00001$; $n = 3$ from 3 biological replicates. (**F**) Representative Western immunoblots of MMP14 and MMP2 in CK-666 treated and shMyo10-silenced human TM cells compared to their respective controls. Densitometry of $n = 4$ immunoblots from three biological replicates for each treatment. $^{*}P = 0.041$, $^{**}P = 0.001$.

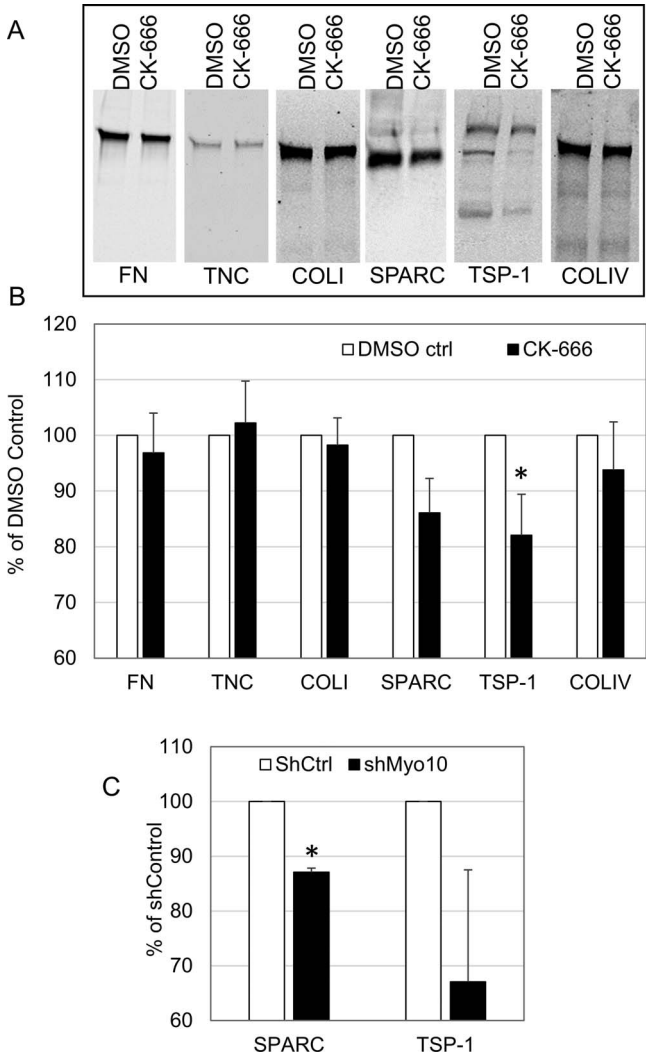

FIGURE 4. ECM protein levels after CK-666 and shMyo10 treatment in TM cells. (**A**) Representative Western immunoblots of FN, TNC collagen type I (COLI), SPARC, TSP-1, and collagen type IV (COLIV) in human TM cell medium after 24 hours of CK-666 or DMSO (vehicle) treatment. (**B**) Densitometry of Westerns ($n = 4$ from three biological replicates) for each protein. *Error bars* are the SEM. $^{*}P < 0.05$ by ANOVA. (**C**) Densitometry of Western immunoblots for SPARC and TSP-1 following shMyo10 silencing. *Error bars* are the SEM; $n = 3$ from three biological replicates. $^{*}P = 0.0005$ by ANOVA.

treatments. First, the outflow rates took longer to occur in Myo10-silenced cells (e.g., at 4 hours, normalized flow rates were 0.7 and 0.55 µl/min in shMyo10-silenced and CK-666-treated anterior segments, respectively). This is likely due to the time that the lentivirus needs to enter the cell and cause an effect compared to the rapid uptake of the reversible CK-666 inhibitor. However, by 75 hours, both treatments led to a similar decrease of 0.6 µl/min. Second, CK-666 caused a biphasic response in outflow compared to Myo10 silencing. The initial decrease (0–4 hours) is likely due to a relatively rapid effect of CK-666 on the actin cytoskeleton. Previously, we showed that actin stress fibers appeared thicker in CK-666-treated TM cells.[13] This suggests that CK-666 caused actin to become stabilized into stress fibers, which is consistent with the observed decrease in outflow at 0 to 4 hours. CK-666 is a reversible inhibitor so, not surprisingly, the outflow rates then recovered to near baseline. We hypothesized that the second decrease in outflow was due to ECM remodeling. Alterations to actin cytoskeleton dynamics can be transmitted to the ECM via integrins, which is known as inside-out signaling or, alternatively, can activate signaling pathways in TM cells to trigger

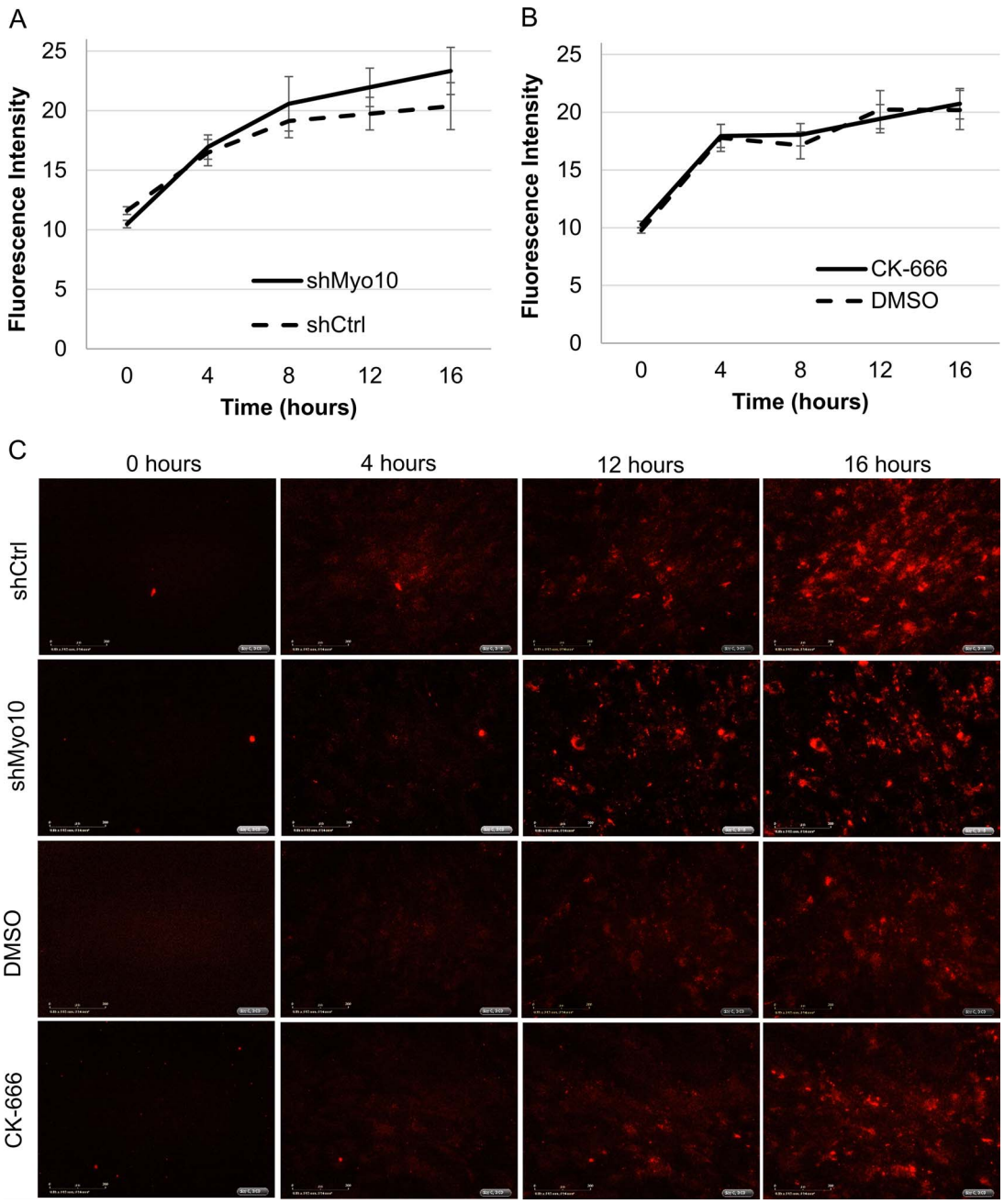

Figure 5. Phagocytosis assay in shMyo-silenced and CK-666-treated TM cells. TM cells were imaged for 16 hours by the Incucyte ZOOM in the presence of opsonized pHrodo Red *S. aureus* bBioparticles. Fluorescence intensity was measured in (**A**) shMyo10-silenced and (**B**) CK-666-treated TM cells compared to their relevant controls ($n = 27$ from $n = 3$ biological replicates). *Error bars* are the SEM. (**C**) Representative images from the phagocytosis assay at 0, 4, 12, and 16 hours after application of the pHrodo bioparticles.

ECM degradation, synthesis, or reorganization of the ECM components of the outflow resistance.[44,46,47] Thus, we tested whether CK-666 affected ECM turnover. MMP activity was significantly reduced in the medium of both shMyo10-silenced and CK-666 treated TM cells. Because TM cells continually release MMPs to remodel ECM in the outflow channels to prevent build-up of cellular debris and ECM fragments,[1] reduced MMP activity may lead to partial obstruction of the outflow channels and the observed decrease in outflow rates in perfusion culture. Finally, we used two different methods targeting two different molecules to inhibit filopodia/TNTs, but it remains possible that Arp2/3 inhibition or Myo10-silencing may produce off-target effects that lead to a decrease in outflow.

Concomitant with altered ECM degradation, we found that SPARC and TSP-1 levels were reduced by CK-666 treatment. Both of these proteins are known to play roles in ECM structural organization. However, in knockout mice, ablation of SPARC and TSP-1 caused lower IOPs (i.e., increased outflow) compared to wild-type littermates.[48,49] These apparent contradictory results may reflect transient (24 hours) versus long-term (months) effects, species differences, or experimental design. It also remains possible that additional ECM proteins are being affected. However, our results are consistent with rapid effects on the actin cytoskeleton at 0 to 4 hours, followed

Investigative Ophthalmology & Visual Science

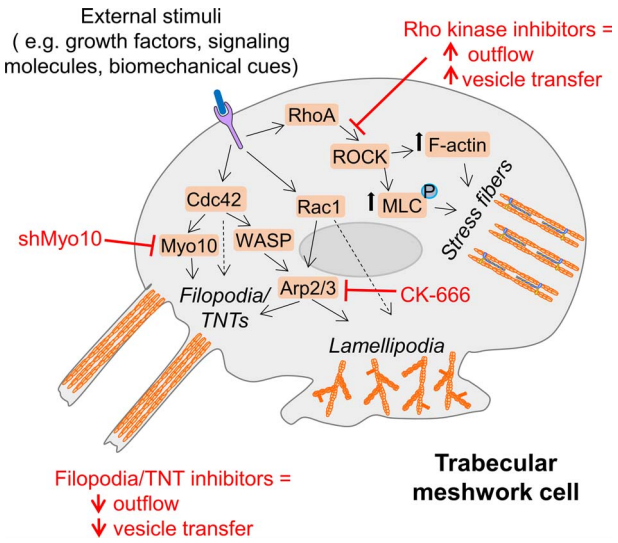

Figure 6. Schematic of the actin cytoskeleton of a TM cell summarizing data found in this study as well as that found in the literature. Inhibiting filopodia/TNTs by shMyo10 silencing lentivirus or CK-666 inhibition of the Arp2/3 complex decreases outflow and reduces vesicle transfer via TNTs. Conversely, relaxing actin stress fiber formation using Rho kinases inhibitors increases outflow and vesicle transfer via TNTs.[13]

by reduced ECM degradation via MMPs, and changes to the composition of the replacement ECM at >48 hours in shMyo10-silenced and CK-666-treated TM.

There are contradictory reports on the role of Myo10 in phagocytosis.[24,26] The original study described that Myo10 is recruited to phagocytic cups and its inhibition resulted in impaired phagocytosis of immunoglobulin G (IgG)-coated beads.[26] However, a later study measured phagocytosis of IgG-coated polystyrene beads or zymosan particles in macrophages derived from Myo10 knockout mice.[24] Their results showed no significant difference in phagocytic uptake between wild-type and Myo10-deficient macrophages. Our results are consistent with this latter study because there was no apparent difference in uptake of *S. aureus* pHrodo bioparticles in shMyo10-silenced or CK-666-treated TM cells. However, phagocytic uptake is dependent on the identity of the ingested particle.[50,51] Thus, variations in type of particle used (*Escherichia coli*, zymosan, and polystyrene beads) and size (2 μm versus 6 μm) could also explain the apparent discrepancies between the study results. Although we did not detect a difference in phagocytic uptake, our results do not preclude the possibility of a role for Myo10 in phagosome transport following engulfment by TM cells.

The schematic in Figure 6 summarizes our results and the current knowledge of the actin cytoskeleton in IOP regulation and cellular communication via TNTs. Prior studies showed that Rho kinase inhibition led to increased outflow through the conventional outflow pathway.[4–7,11] Recently, we showed that the Rho kinase inhibitor Y27632 increased vesicle transfer via TNT, whereas, conversely, CK-666 treatment reduced vesicle transfer and filopodia number and length.[13] In this study, we found that two methods of targeting filopodia and TNTs caused reduction in outflow rates via the TM. Together, our results show that Myo10 plays a role in outflow regulation both via its regulation of actin-based filopodia/TNTs as well as downstream effects on ECM turnover. These results provide additional insight into the role of the actin cytoskeleton in the outflow pathway.

Acknowledgments

The authors thank Lions VisionGift (Portland, OR, USA) for facilitating the procurement of human cadaver eyes.

Supported by NIH/NEI grants EY019643 (KEK), EY010572 (P30 Casey Eye Institute Core facility grant), and an unrestricted grant to the Casey Eye Institute from Research to Prevent Blindness (New York, NY, USA).

Disclosure: **Y.Y. Sun**, None; **Y.-F. Yang**, None; **K.E. Keller**, None

References

1. Keller KE, Acott TS. The juxtacanalicular region of ocular trabecular meshwork: a tissue with a unique extracellular matrix and specialized function. *J Ocular Biol*. 2013;1:10.
2. Quigley HA. Glaucoma. *Lancet*. 2011;377:1367–1377.
3. Nobes CD, Rho, Hall A. rac and cdc42 GTPases: regulators of actin structures, cell adhesion and motility. *Biochem Soc Trans*. 1995;23:456–459.
4. Rao PV, Deng PF, Kumar J, Epstein DL. Modulation of aqueous humor outflow facility by the Rho kinase-specific inhibitor Y-27632. *Invest Ophthalmol Vis Sci*. 2001;42:1029–1037.
5. Vittitow JL, Garg R, Rowlette LL, Epstein DL, O'Brien ET, Borras T. Gene transfer of dominant-negative RhoA increases outflow facility in perfused human anterior segment cultures. *Mol Vis*. 2002;8:32–44.
6. Rao PV, Pattabiraman PP, Kopczynski C. Role of the Rho GTPase/Rho kinase signaling pathway in pathogenesis and treatment of glaucoma: bench to bedside research. *Exp Eye Res*. 2017;158:23–32.
7. Kaufman PL, Rasmussen CA. Advances in glaucoma treatment and management: outflow drugs. *Invest Ophthalmol Vis Sci*. 2012;53:2495–2500.
8. Peterson JA, Tian B, Bershadsky AD, et al. Latrunculin-A increases outflow facility in the monkey. *Invest Ophthalmol Vis Sci*. 1999;40:931–941.
9. Rasmussen CA, Kaufman PL, Ritch R, Haque R, Brazzell RK, Vittitow JL. Latrunculin B reduces intraocular pressure in human ocular hypertension and primary open-angle glaucoma. *Trans Vis Sci Tech*. 2014;3(5):1.
10. Tian B, Gabelt BT, Geiger B, Kaufman PL. The role of the actomyosin system in regulating trabecular fluid outflow. *Exp Eye Res*. 2009;88:713–717.
11. Inoue T, Tanihara H. Rho-associated kinase inhibitors: a novel glaucoma therapy. *Prog Retin Eye Res*. 2013;37:1–12.
12. Kazemi A, McLaren JW, Kopczynski CC, Heah TG, Novack GD, Sit AJ. The effects of netarsudil ophthalmic solution on aqueous humor dynamics in a randomized study in humans. *J Ocul Pharmacol Ther*. 2018;34:380–386.
13. Keller KE, Bradley JM, Sun YY, Yang YF, Acott TS. Tunneling nanotubes are novel cellular structures that communicate signals between trabecular meshwork cells. *Invest Ophthalmol Vis Sci*. 2017;58:5298–5307.
14. Mattila PK, Lappalainen P. Filopodia: molecular architecture and cellular functions. *Nat Rev Mol Cell Biol*. 2008;9:446–454.
15. Rotty JD, Wu C, Bear JE. New insights into the regulation and cellular functions of the ARP2/3 complex. *Nat Rev Mol Cell Biol*. 2013;14:7–12.
16. Gurke S, Barroso JF, Gerdes HH. The art of cellular communication: tunneling nanotubes bridge the divide. *Histochem Cell Biol*. 2008;129:539–550.
17. Gerdes HH, Rustom A, Wang X. Tunneling nanotubes, an emerging intercellular communication route in development. *Mech Dev*. 2013;130:381–387.
18. Rustom A, Saffrich R, Markovic I, Walther P, Gerdes HH. Nanotubular highways for intercellular organelle transport. *Science*. 2004;303:1007–1010.

19. Gousset K, Marzo L, Commere PH, Zurzolo C. Myo10 is a key regulator of TNT formation in neuronal cells. *J Cell Sci*. 2013; 126:4424–4435.
20. Bohil AB, Robertson BW, Cheney RE. Myosin-X is a molecular motor that functions in filopodia formation. *Proc Natl Acad Sci U S A*. 2006;103:12411–12416.
21. Kerber ML, Cheney RE. Myosin-X: a MyTH-FERM myosin at the tips of filopodia. *J Cell Sci*. 2011;124:3733–3741.
22. Sousa AD, Cheney RE. Myosin-X: a molecular motor at the cell's fingertips. *Trends Cell Biol*. 2005;15:533–539.
23. Watanabe TM, Tokuo H, Gonda K, Higuchi H, Ikebe M. Myosin-X induces filopodia by multiple elongation mechanism. *J Biol Chem*. 2010;285:19605–19614.
24. Horsthemke M, Bachg AC, Groll K, et al. Multiple roles of filopodial dynamics in particle capture and phagocytosis and phenotypes of Cdc42 and Myo10 deletion. *J Biol Chem*. 2017; 292:7258–7273.
25. McMichael BK, Cheney RE, Lee BS. Myosin X regulates sealing zone patterning in osteoclasts through linkage of podosomes and microtubules. *J Biol Chem*. 2010;285:9506–9515.
26. Cox D, Berg JS, Cammer M, et al. Myosin X is a downstream effector of PI(3)K during phagocytosis. *Nat Cell Biol*. 2002;4: 469–477.
27. Arjonen A, Kaukonen R, Mattila E, et al. Mutant p53-associated myosin-X upregulation promotes breast cancer invasion and metastasis. *J Clin Invest*. 2014;124:1069–1082.
28. Cao R, Chen J, Zhang X, et al. Elevated expression of myosin X in tumours contributes to breast cancer aggressiveness and metastasis. *Br J Cancer*. 2014;111:539–550.
29. Luna C, Li G, Liton PB, Epstein DL, Gonzalez P. Alterations in gene expression induced by cyclic mechanical stress in trabecular meshwork cells. *Mol Vis*. 2009;15:534–544.
30. Tasca A, Astleford K, Lederman A, et al. Regulation of osteoclast differentiation by myosin X. *Sci Rep*. 2017;7:7603.
31. Zhang H, Berg JS, Li Z, et al. Myosin-X provides a motor-based link between integrins and the cytoskeleton. *Nat Cell Biol*. 2004;6:523–531.
32. Hetrick B, Han MS, Helgeson LA, Nolen BJ. Small molecules CK-666 and CK-869 inhibit actin-related protein 2/3 complex by blocking an activating conformational change. *Chem Biol*. 2013;20:701–712.
33. Nolen BJ, Tomasevic N, Russell A, et al. Characterization of two classes of small molecule inhibitors of Arp2/3 complex. *Nature*. 2009;460:1031–1034.
34. Keller KE, Bhattacharya SK, Borras T, et al. Consensus recommendations for trabecular meshwork cell isolation, characterization and culture. *Exp Eye Res*. 2018;171:164–173.
35. Keller KE, Bradley JM, Vranka JA, Acott TS. Segmental versican expression in the trabecular meshwork and involvement in outflow facility. *Invest Ophthalmol Vis Sci*. 2011;52: 5049–5057.
36. Keller KE, Sun YY, Yang YF, Bradley JM, Acott TS. Perturbation of hyaluronan synthesis in the trabecular meshwork and the effects on outflow facility. *Invest Ophthalmol Vis Sci*. 2012; 53:4616–4625.
37. Erickson-Lamy K, Rohen JW, Grant WM. Outflow facility studies in the perfused human ocular anterior segment. *Exp Eye Res*. 1991;52:723–731.
38. Keller KE, Bradley JM, Acott TS. Differential effects of ADAMTS-1, -4, and -5 in the trabecular meshwork. *Invest Ophthalmol Vis Sci*. 2009;50:5769–5777.
39. Keller KE, Bradley JM, Kelley MJ, Acott TS. Effects of modifiers of glycosaminoglycan biosynthesis on outflow facility in perfusion culture. *Invest Ophthalmol Vis Sci*. 2008;49: 2495–2505.
40. Keller KE, Yang YF, Sun YY, et al. Interleukin-20 receptor expression in the trabecular meshwork and its implication in glaucoma. *J Ocul Pharmacol Ther*. 2014;30:267–276.
41. Aga M, Bradley JM, Wanchu R, Yang YF, Acott TS, Keller KE. Differential effects of caveolin-1 and -2 knockdown on aqueous outflow and altered extracellular matrix turnover in caveolin-silenced trabecular meshwork cells. *Invest Ophthalmol Vis Sci*. 2014;55:5497–5509.
42. Aga M, Bradley JM, Keller KE, Kelley MJ, Acott TS. Specialized podosome- or invadopodia-like structures (PILS) for focal trabecular meshwork extracellular matrix turnover. *Invest Ophthalmol Vis Sci*. 2008;49:5353–5365.
43. Linder S, Kopp P. Podosomes at a glance. *J Cell Sci*. 2005;118: 2079–2082.
44. Keller KE, Aga M, Bradley JM, Kelley MJ, Acott TS. Extracellular matrix turnover and outflow resistance. *Exp Eye Res*. 2009;88:676–682.
45. Acott TS, Kelley MJ. Extracellular matrix in the trabecular meshwork. *Exp Eye Res*. 2008;86:543–561.
46. Vranka JA, Kelley MJ, Acott TS, Keller KE. Extracellular matrix in the trabecular meshwork: intraocular pressure regulation and dysregulation in glaucoma. *Exp Eye Res*. 2015;133:112–125.
47. Gagen D, Faralli JA, Filla MS, Peters DM. The role of integrins in the trabecular meshwork. *J Ocul Pharmacol Ther*. 2014; 30:110–120.
48. Haddadin RI, Oh DJ, Kang MH, et al. Thrombospondin-1 (TSP1)-null and TSP2-null mice exhibit lower intraocular pressures. *Invest Ophthalmol Vis Sci*. 2012;53:6708–6717.
49. Haddadin RI, Oh DJ, Kang MH, et al. SPARC-null mice exhibit lower intraocular pressures. *Invest Ophthalmol Vis Sci*. 2009; 50:3771–3777.
50. Porter KM, Epstein DL, Liton PB. Up-regulated expression of extracellular matrix remodeling genes in phagocytically challenged trabecular meshwork cells. *PLoS One*. 2012;7: e34792.
51. Paul D, Achouri S, Yoon YZ, Herre J, Bryant CE, Cicuta P. Phagocytosis dynamics depends on target shape. *Biophys J*. 2013;105:1143–1150.

Investigative Ophthalmology & Visual Science